NANO LETTERS

2008
Vol. 8, No. 9
2794-2799

Structure and Cathodoluminescence of Individual ZnS/ZnO Biaxial Nanobelt Heterostructures

Jian Yan,[†] Xiaosheng Fang,*[,†,‡,§] Lide Zhang,*[,†] Yoshio Bando,[‡] Ujjal K. Gautam,*[,‡] Benjamin Dierre,[||] Takashi Sekiguchi,[||] and Dmitri Golberg[‡,§]

Key Laboratory of Materials Physics, and Anhui Key Laboratory of Nanomaterials and Nanostructures, Institute of Solid State Physics, Chinese Academy of Sciences, Hefei 230031, People's Republic of China, and Nanoscale Materials Center, Advanced Electronic Materials Center, and World Premier International Center for Materials Nanoarchitectonics, National Institute for Materials Science, Namiki 1-1, Tsukuba, Ibaraki 305-0044, Japan

Received May 12, 2008; Revised Manuscript Received June 30, 2008

ABSTRACT

We report on a controlled synthesis of two novel semiconducting heterostructures: heterocrystalline-ZnS/single-crystalline-ZnO biaxial nanobelts and side-to-side single-crystalline ZnS/ZnO biaxial nanobelts via a simple one-step thermal evaporation method. In the first heterostructure, a ZnS domain is composed of the heterocrystalline superlattice $(3C\text{-}ZnS)_N/(2H\text{-}ZnS)_M$[111]-[0001] with the atomically smooth interface between wurtzite and zinc blende ZnS fragments. High-spatial resolution cathodoluminescence studies on individual heterostructures for the first time reveal a new ultraviolet emission peak (~355 nm), which is not observed in separate ZnS or ZnO nanostructures. The present hererostructures are expected to become valuable not only with respect to fundamental research but also for a design of new broad-range ultraviolet nanoscale lasers and sensors.

Since the beginning of 2002, three leading groups have been systematically exploring how to bring out new functional properties from a single nanowire.[1−3] By alternating vaporization of two materials during the vapor−liquid−solid (VLS) growth, they have grown striped "superlattice" nanowires or heterostructures.[4] One-dimensional (1D) nano/heterostructures consisting of two important functional materials are of prime importance for revealing unique properties and essential for developing potential nanoelectronic and optoelectronic devices.[5−16] For example, GaAs/GaP nanowire superlattices are demonstrated to be suitable candidates for fabricating nanophotonic devices,[1] whereas InAs/InP radial nanowire heterostructures are effective in high electron mobility devices.[17] The fabrication of these structures are characterized by concomitant growth enabling mutual lattice tuning of the constituents and thus reducing the hardship of interface electron scattering and enhancing device performances.

ZnO and ZnS, well-known direct band gap II−VI semiconductors, are promising materials for fabricating photonic, optical, and electronic devices. With wide band gaps of ~3.37 eV, 3.72 eV and ~3.77 eV for ZnO, cubic zinc blende (ZB), and hexagonal wurtzite (WZ) ZnS, respectively, heterostructures of these compounds are unique candidates for ultraviolet lasers and detectors working in the 320−400 nm wavelength range, naturally accessible at the earth surface.[18−21] Recently, Schrier and co-workers used theoretical calculations to determine the optical properties of ZnO/ZnS heterostructures and proposed that they should be used for potential photovoltaic devices.[22] However, the synthesis of ZnO/ZnS heterostructures or biaxial nanostructures has been a challenge until date. This is mainly due to the high sensitivity of such heterostructures to synthetic conditions, such as, oxidation propensity of ZnS surfaces as well as differential solubility of the constituents in the catalyst particle.

Being motivated by the encouraging theoretical predictions as well as a rare possibility to merge these two important optical materials, we have systematically investigated the growth and structure of 1D heterostructures composed of

* To whom correspondence should be addressed. E-mail: xsfang@issp.ac.cn (X.S.F.); ldzhang@issp.ac.cn (L.D.Z.); Gautam.Ujjal@nims.go.jp (U.K.G.). Fax: (+86) 551-559-1434.

[†] Chinese Academy of Sciences.

[‡] World Premier International Center for Materials Nanoarchitectonics, National Institute for Materials Science.

[§] Nanoscale Materials Center, National Institute for Materials Science.

[||] Advanced Electronic Materials Center, National Institute for Materials Science.

10.1021/nl801353c CCC: $40.75
Published on Web 08/08/2008

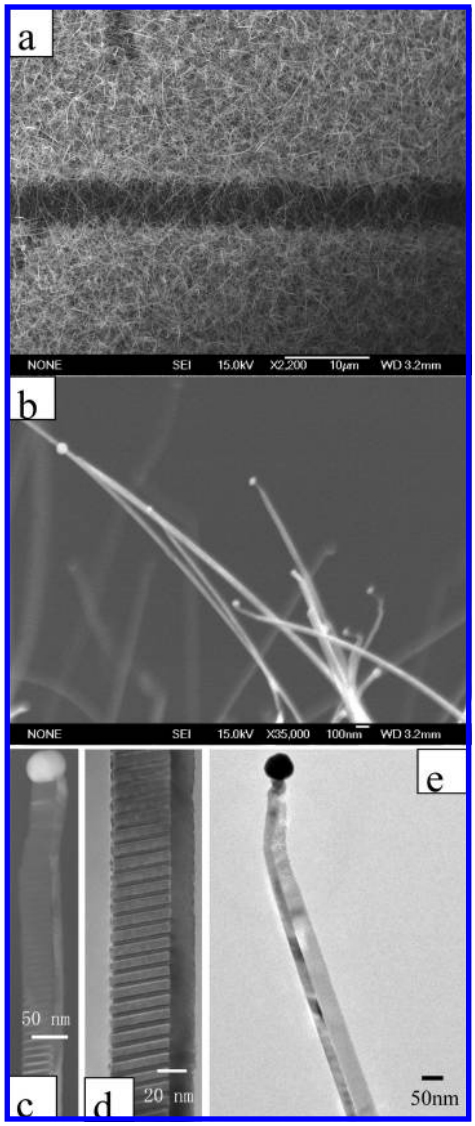

Figure 1. (a,b) Low- and high-magnification SEM micrographs of the as-grown products. (c,d) Typical TEM images of heterocrystalline ZnS/ single-crystalline-ZnO biaxial nanobelts. (e) A TEM image of a side-to-side single-crystalline ZnS/ZnO biaxial nanobelts.

II−VI and II−VI semiconductors. Furthermore, we have also explored the novel excitonic properties of these structures owing to an epitaxial interface by employing high resolution cathodoluminescence (CL) spectroscopy. Thus, here is a report on the controlled fabrication of two novel heterostructures: heterocrystalline-ZnS/single-crystalline-ZnO biaxial nanobelts and side-to-side single-crystalline ZnS/ZnO biaxial nanobelts through a simple thermal evaporation method using gold as catalyst. Detailed structural analysis was performed that gave vital clues to understand the nanostructure growth mechanism. The CL properties were analyzed at 293 K and ∼30 K. These were nearly identical for both heterostructures, notably while a novel ultraviolet emission peak centered at ∼355 nm was observed for the first time along with normal ZnS or ZnO band-edge emissions.

The synthesis of the ZnS/ZnO biaxial nanobelt heterostructures was carried out in a conventional horizontal furnace. In brief, an alumina tube (outer diameter, 25 mm; length, 80 cm) was mounted horizontally inside a single-zone high temperature resistance furnace. A 0.3 g sample of commercially available ZnS powder (99.99% purity) was used as a source material. It was placed in the center of the heating zone. A Si (100) substrate coated with a 1.5 nm thick Au film was vertically put downstream of ZnS powders at a distance of 11 cm (∼950 °C). Before heating, the system was purged with 80 sccm (standard cubic centimeter per minute) high-purity argon (Ar, 99.999%) for 1 h. Then, the furnace was heated to 1100 °C in 10 min and kept at this temperature for 10 min with the Ar flow keeping constant. After the system was cooled down to room temperature, a white-colored wool-like product was found deposited onto the silicon substrate.

The as-synthesized products were characterized using a field-emission scanning electron microscope (FESEM, Sirion 200 and JSM-6700F) and a high-resolution transmission electron microscope (HRTEM, JEOL 2010 and JEM-3000F) equipped with an X-ray energy dispersive spectrometer (EDS).

Figure 1a is a low-magnification SEM image of the product. The product is composed of nanostructures with diameters varying from several tens of nanometers to 100 nm and lengths up to tens of micrometers. A high-magnification SEM image of the product is depicted in Figure 1b. Each nanostructure has a nanoparticle on its tip end. Further investigations by TEM and EDS suggest that most of the products are composed of either of two heterostructures: heterocrystalline ZnS/single-crystalline-ZnO biaxial nanobelts or side-to-side single-crystalline ZnS/ZnO biaxial nanobelts. Besides those, a few pure single-crystalline ZnS nanobelts have also been observed. The TEM images of two types of biaxial nanobelts are displayed in Figure 1c−e. The clear and uniform interfaces are visible along the nanostructures. The left side layers of the nanobelts in Figure 1c,d display sequential dark/light contrast strips, indicating that they have a periodically modulated structure. A distinct interface between the two parallel layers can be seen. The structure is somewhat similar to the recently reported side-to-side biaxial nanostructures.[23−25]

A detailed chemical analysis was carried out using elemental mappings and EDS. Figure 2a shows a typical TEM image of a side-to-side single-crystalline ZnS/ZnO biaxial nanobelt, which reveals the clear and uniform interface between the upper ZnS fragment and the lower ZnO fragment. The individual diameters are ∼40 nm and ∼30 nm for ZnS and ZnO domains, respectively. The elemental maps displayed in Figure 2b−d shed light on the distribution of the constituting elements, that is, Zn, S, and O. These clearly demonstrate a well-defined compositional profile of the ZnS/ZnO biaxial nanobelt. On the basis of TEM images, it should be noted that the interface region (both in Figure 1e and in Figure 2a) appears to have a thin region with a brighter contrast. We investigated this region for a possible detection of a third phase, such as metallic Zn. It was found that, even though it might be fuzzy at some places (see Supporting Information Figure S1), the interface is normally

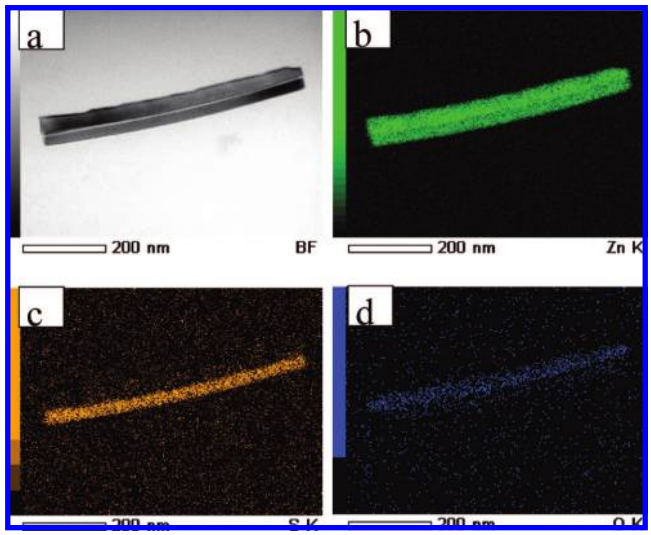

Figure 2. (a) Typical TEM image of a side-to-side single-crystalline ZnS/ZnO biaxial nanobelt revealing a clear and uniform interface between two structures. (b−d) The Zn, S, and O elemental maps demonstrating well-defined compositional profiles within the nanobelt.

distinct and the presence of a third phase is outside the detection limits of the instrument.

Figure 3a shows a typical TEM image of heterocrystalline ZnS/ single-crystalline-ZnO biaxial nanobelt, revealing ZnO and ZnS subnanobelts of uniform diameters along their axes. The EDS spectra in Figure 3b−d were taken from the marked parts of the biaxial nanobelt, as shown in Figure 3a. These supported the results of the elemental mappings. The highly crystalline nature of these two novel heterostructures was further verified by selected area electron diffraction (SAED) and HRTEM. Figure 3e is a corresponding SAED pattern of the heterocrystalline ZnS/single-crystalline-ZnO biaxial nanobelt, previously shown in Figure 3a. It is composed of three sets of diffraction spots. One of them can be indexed to WZ ZnO, as indicated by a small rectangle; the others can be indexed to ZB and WZ ZnS, as marked by a dashed hexagon and a large rectangle, respectively. The regarded structures are illustrated in the HRTEM images (Figure 3f,g) taken from the ZnO and ZnS fragments, respectively. In Figure 3f, the marked interplanar *d* spacings are ∼0.52 nm and ∼0.28 nm. These correspond to the (0001) and (01$\bar{1}$0) lattice planes of WZ ZnO, respectively. In Figure 3g, it can be seen that the ZnS portion is composed of two kinds of lattices. The marked interplanar *d* spacing (∼0.31 nm) corresponds to that of the {111} lattice planes of ZB ZnS, and the distances of ∼0.63 nm and ∼0.33 nm correspond to the (0001) and (01$\bar{1}$0) lattice planes of WZ ZnS, respectively. Thus, the ZnS portion has the heterocrystalline superlattice structure $(3C-ZnS)_N/(2H-ZnS)_M$[111]-[0001], where *N* and *M* are the numbers of the atomic layers in the ZB and WZ ZnS sections. These usually vary from 9 to 11 and from 24 to 28, respectively. The interface between the WZ ZnS and the ZB ZnS sections is atomically smooth.

The abrupt interfaces of WZ-ZnS/ZnO and ZB-ZnS/ZnO are depicted in Figure 3h, and marked with I1 and I2, respectively. The I1 interface is ∼8.2 nm long and parallel

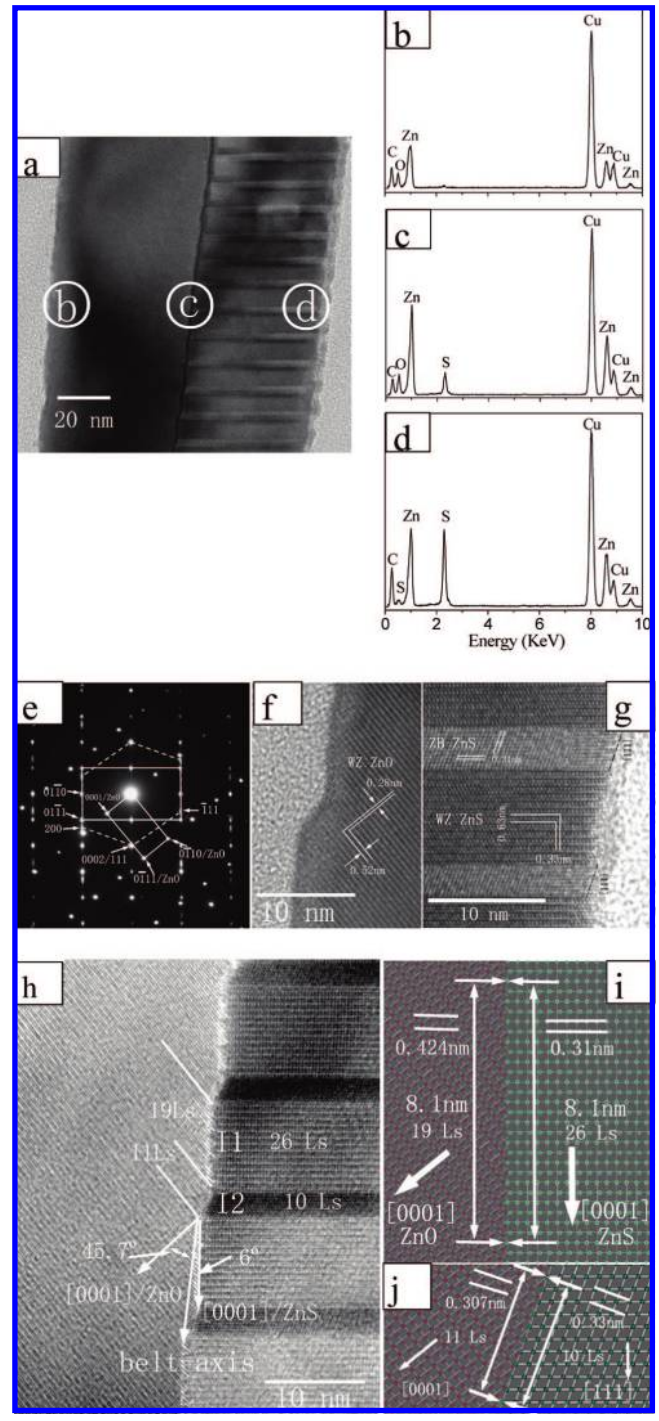

Figure 3. (a) High-magnification TEM image of the ZnS/ZnO biaxial nanobelts. (b−d) The EDS spectra taken from the labeled regions. (e) The corresponding SAED pattern of the ZnS/ZnO biaxial nanobelt shown in (a) (the incident electron beam is parallel to [2$\bar{1}\bar{1}$0]/ZnO, [2$\bar{1}$$\bar{1}$0]/WZ-ZnS, and [01$\bar{1}$]/ZB-ZnS). (f) HRTEM image recorded from a single-crystalline ZnO fragment. (g) HRTEM image taken from a ZnS fragment displaying the heterocrystalline superlattices. (h) HRTEM image of the ZnS/ZnO interface. (i) A structural model of the WZ-ZnS/ZnO interface marked with "I1" in (h). (j) A structural model of the ZB-ZnS/ZnO interface marked with "I2" in (h).

to the (01$\bar{1}$0) plane of WZ ZnS. The structure model of the I1 interface is shown in Figure 3i. Along the I1 interface, the lattice constant of the ZnS side is ∼0.31 nm and that of the ZnO side is ∼0.424 nm. The length of 26 layers (Ls) on

the ZnS side ($26 \times 0.31 = 8.06$ nm) is approximately equal to the distance of 19 Ls on the ZnO side ($19 \times 0.424 = 8.056$ nm). This value is coincident with the measured distance of the I1 interface. The lattice mismatch between the WZ ZnS and the ZnO is ~36.7%. This causes the asymmetric stresses in various domains: tension in the ZnS side and compression in the ZnO side. The length limitation of the I1 interface may be due to these residual stresses. Similar to the I1 interface, a structural model of the I2 interface was constructed, as shown in Figure 3j. The I2 interface is parallel to the $(1\bar{1}\bar{1})$ face of the ZB ZnS and is ~3.3 nm in length. Along the I2 interface, the lattice constant of the ZnO side is ~0.307 nm and that of the ZnS side is ~0.33 nm. This means that the asymmetric residual stresses caused by the I2 interface, that is, tension in the ZnO side and compression in the ZnS side, are opposite in sign to those of the I1 interface. The alternating growth of I1 and I2 interfaces might reduce the stresses and system energy. This leads to the formation of heterocrystalline-ZnS/single-crystalline-ZnO biaxial nanobelts, and they remain stable.

It is important to point out that the belt axes are not parallel to the *c* axis of the WZ ZnS section, the [111] direction of ZB ZnS section, or the *c* axis of the ZnO subnanobelt (Figure 3f). An angle between the belt axis and the [0001] direction of WZ ZnS section is ~6°. Meanwhile, an angle between the belt axis and the [0001] direction of a ZnO subnanobelt is close to 45.7°. It means that the growth of the ZnS and ZnO subnanobelts takes place not along the low-indexed planes. This is an obvious difference from the conventional 1D ZnS and ZnO nanostructures[26−29] and the standard subnanobelts within biaxial nanobelts.[23−25]

The above-mentioned structural characterizations and discussions have mainly been related to the heterocrystalline-ZnS/single-crystalline-ZnO biaxial nanobelts. The TEM images and HRTEM analyses of the relevant side-to-side single-crystalline ZnS/ZnO biaxial nanobelts are demonstrated in Supporting Information (Figures S2 and S3).

During the experiments, we found that Au nanoparticles play an important role in the formation of both heterostructure types. No such products were found in the absence of Au nanoparticles, as verified in Figure 1a. From Figure 1c−e, it can be seen that both ZnS and ZnO portions are attached to the same Au nanoparticle indicating that both fragments grew simultaneously during the experiment. Such growth model is different from the ones previously proposed to explain the formation of biaxial nanostructures in two subsequent processes: the initial growth of one component followed by the epitaxial growth of the secondary component on the template thus formed.[23]

It is well-known that a lattice mismatch strain is widely used to control the nanoscale pattern formation. For example, Wang et al. reported that the asymmetric residual stresses caused by the boundaries in a bicrystal AlN nanowire can lead to the formation of a zigzag morphology.[30] Alivisatos et al. reported the formation of CdS-Ag_2S superlattice nanorods induced by the mismatch strain.[31] Careful experiments employing grazing incidence X-ray techniques have shown that the strain release by the creation of heterostructures can be well-explained with atomistic simulations.[32] In our case, we propose that the formation of ZnS/ZnO biaxial nanobelt heterostructures during a vapor−liquid−solid (VLS) process is a direct result of the asymmetric residual stresses. The ZnS and ZnO vapors (since no oxygen source was utilized during the synthesis process, the formation of ZnO vapor should be due to the presence of residual oxygen in the reaction system) were transported and absorbed by an Au nanoparticle. When the alloy droplet became supersaturated, ZnS and ZnO were phase-separated and nucleated to form heterostructures. Because of a large lattice mismatch between ZnS and ZnO, the effect of mismatch strain is considerably important. Taking the ZnS/ZnO biaxial nanobelt as an example, we note that the mismatch strain at the ZnS and ZnO interface can increase the system energy. Accordingly, the morphology and/or crystal structure of a ZnS/ZnO biaxial nanobelt need to be adopted to reduce the mismatch strain energy. Experimentally, we observed two kinds of changes. One is curving of a ZnS/ZnO biaxial nanobelt that preserves the single-crystalline appearance of ZnS and ZnO parts. The other one is periodic crystal structure alternating (WZ ↔ ZB) within a ZnS subnanobelt, while the whole structure remains straight (the phase transformation and stacking fault energies are both low in ZnS presuming a relative ease of such process).[27]

In order to investigate the optical properties of novel heterostructures, cathodoluminescence (CL) from individual objects was performed at a high-spatial resolution at room (RT) and low temperature (LT, ~30 K). The RT CL spectra from individual structures were collected with a high-resolution CL system using an accelerating voltage of 5 kV and a current of 1000 pA. An ultra-high vacuum scanning electron microscope (UHV-SEM) with a Gemini electron gun (Omicron, Germany) equipped with a CL system was utilized.[33] The RT and LT CL measurements implied that two heterostructure types had almost the same CL properties. Figure 4b depicts typical CL spectra obtained at RT from an individual heterocrystalline-ZnS/single-crystalline-ZnO biaxial nanobelt. The corresponding SEM image is shown in Figure 4a. The RT CL spectra (Figure 4b) were taken in different spots marked as 1 and 2 in Figure 4a. The EDS spectra and TEM observations confirmed that the present structure consists of two parts: (1) pure ZnS and (2) pure ZnO. The CL spectra reveal a broad visible emission band centered at ~535 nm and a weak sharp ultraviolet emission band centered at ~345 or ~385 nm. Figure 4c is an enlarged portion of the sharp ultraviolet emission bands between 310−430 nm. In the ultraviolet region, it is easy to see that curve 1 is composed of a very weak sharp ultraviolet emission band centered at ~345 nm, while a little stronger and sharp ultraviolet emission band centered at ~385 nm is apparent for curve 2. These observations are consistent with an expected half-ZnS and half-ZnO morphology (see Supporting Information, Figure S4, for CL images of the individual components).

The CL spectra measured at low temperature (LT) show distinct near band-edge emissions. Such measurements were carried out using a high spatial resolution (~50 nm) and a

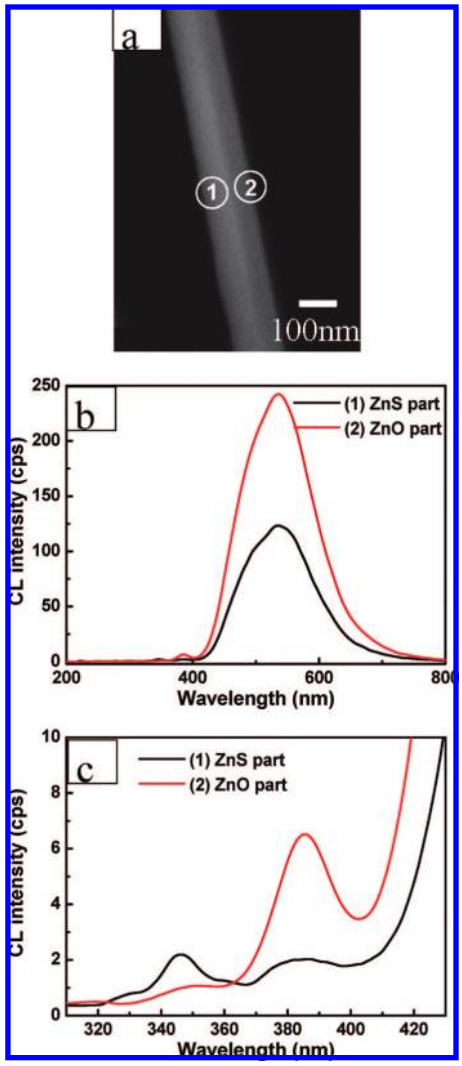

Figure 4. (a) SEM image of ZnS/ZnO biaxial nanobelts. (b) CL spectra recorded at RT from the marked regions in (a). (c) The enlarged portion of the sharp ultraviolet emission bands in (b) between 310 and 430 nm.

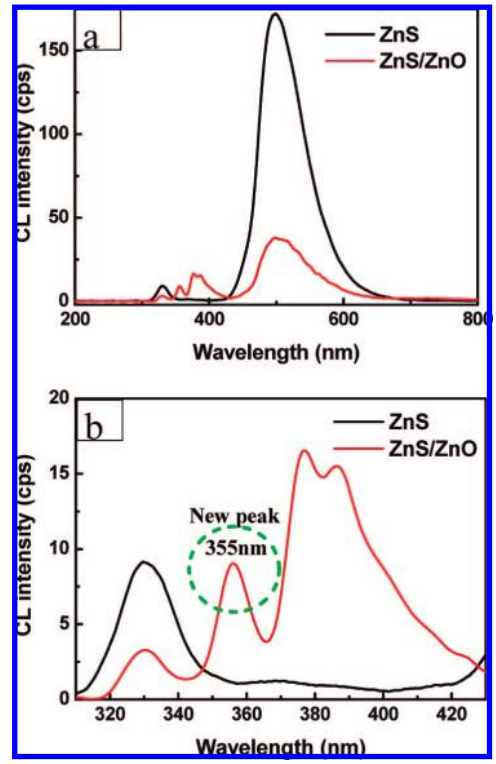

Figure 5. (a) Representative CL spectra obtained at ~30 K from individual ZnS/ZnO biaxial nanobelts and pure ZnS nanobelts. (b) Corresponding enlarged view of the near band-edge emissions between 310 to 430 nm. A new ultraviolet emission peak (~355 nm) is observed for individual ZnS/ZnO biaxial nanobelts which is absent either in the pure 1D ZnS or in the ZnO nanostructures.

low-energy CL (HRLE-CL) system and a thermal field-emission scanning electron microscope (TFE-SEM, Hitachi S4200).[23] Figure 5 displays two representative CL spectra obtained at ~30 K from an individual heterocrystalline-ZnS/single-crystalline-ZnO biaxial nanobelt and a pure ZnS nanobelt, and the corresponding enlarged portions of the near band-edge emissions between 310 to 430 nm. The typical CL spectrum of an individual ZnS/ZnO biaxial nanobelt at ~30 K exhibits a broad and strong visible emission band centered at ~501 nm and 4 weak ultraviolet emission bands centered at ~330, 355, 376, and 386 nm. In comparing with pure ZnS or ZnO nanostructures, a new ultraviolet emission peak (~355 nm) is found, which has not been observed at RT for the same nanobelt.

The research on optical properties of 1D ZnO and ZnS nanostructures has rapidly expanded in recent years and visible emissions centered mainly at 400−650 nm and the band-edge emission (ultraviolet region, ~368−390 nm for ZnO, ~330−345 nm for ZnS) at RT or LT have been documented.[21,34−36] The possible reason behind the variations in the position of band-edge emissions in ZnO nanostructures (of different sizes) is the concentration of native defects. The visible emissions in the present experiments mainly originate from some self-activated centers, for example, vacancy states, singly ionized vacancies, interstitial and/or surface states, and so forth[37−39] (e.g., such as excessive elemental S and O detected in the EDS spectra, Figure 3b,d).

In the ultraviolet region, along with normal ultraviolet emissions originated from band-edge luminescence of ZnS or ZnO,[21,34−36,40,41] a new ultraviolet emission peak centered at ~355 nm was observed. Such a peak has never been seen before for any standard 1D ZnS and/or ZnO nanostructure (Figure 5b). On the basis of the EDS data in Figure 3b, in which O is excessive and the atomic ratio between O and S is close to ~2:1, the structural characterizations, and LT CL spectra, this new ultraviolet emission peak (~355 nm) could be assigned to the presence of an interface ZnS/ZnO structure. A Zn−O−S ternary phase or an oxygen-doped ZnS nanostructure presumably exists in this region. The effect of oxygen on ZnS or ZnSe band structures and optical properties has recently been experimentally and theoretically investigated.[42,43] Such effect may shed light on the new peak origin. An extensive work, such as fabrication and optical analysis of larger diameter ZnS/ZnO biaxial nanobelts, that make the high-spatial resolution LT CL measurements along the structure axis possible, is underway in order to unambiguously determine the new emission peak nature.

To conclude, two novel ZnS/ZnO biaxial nanobelt heterostructures, namely, heterocrystalline-ZnS/single-crystalline-ZnO biaxial nanobelts and side-to-side single-crystalline ZnS/ZnO biaxial nanobelts, were created via a simple one-step thermal evaporation method. Then their detailed structural analysis was carried out. These interesting geometries resulted in unique cathodoluminescence properties including a new ultraviolet emission peak at ~355 nm observed for the first time in any ZnS and/or ZnO 1D nanostructure. The simple designed method might be useful for the synthesis of diverse heterostructures, such as II−VI or III−V semiconducting composite nanostructures, and the fabricated novel nanomaterials are envisaged to be of high promise for novel optoelectronic nanoscale devices.

Acknowledgment. This work was financially supported by the National Major Project of Fundamental Research: Nanomaterials and Nanostructures (Grant 2005CB23603), the Special fund for President Scholarship, Chinese Academy of Science, the Natural Science Foundation of China (Grant 90406008), and in part by the World Premier International Research Center on Materials Nanoarchitectonics (MANA), MEXT, tenable at NIMS, Japan.

Supporting Information Available: TEM images of several heterostructures at various magnifications, HRTEM image of a region at the interface, dark-field images of the nanostructures showing the ZnO and ZnS phases, CL images of a heterostructure, and TEM and HRTEM images of a side-to-side single-crystalline ZnS/ZnO biaxial nanobelt. This information is available free of charge via the Internet at http://pubs.acs.org.

References

(1) Gudiksen, M. S.; Lauhon, L. J.; Wang, J.; Smith, D. C.; Lieber, C. M. *Nature* **2002**, *415*, 617.
(2) Wu, Y. Y.; Fan, R.; Yang, P. D. *Nano. Lett.* **2002**, *2*, 83.
(3) Bjork, M. T.; Ohlosson, B. J.; Sass, T.; Persson, A. I.; Thelander, C.; Magnusson, M. H.; Deppert, K.; Wallenberg, L. R.; Samuelson, L. *Nano. Lett.* **2002**, *2*, 87.
(4) Lieber, C. M. *Nano. Lett.* **2002**, *2*, 81.
(5) Mieszawska, A. J.; Jalilian, R.; Sumanasekera, G. U.; Zamborini, F. P. *Small* **2007**, *3*, 722.
(6) Zhan, J. H.; Bando, Y.; Hu, J. Q.; Liu, Z. W.; Yin, L. W.; Golberg, D. *Angew. Chem., Int. Ed.* **2005**, *44*, 2140.
(7) Hu, J. Q.; Bando, Y.; Zhan, J. H.; Golberg, D. *Adv. Mater.* **2005**, *17*, 1964.
(8) Xia, Y. N.; Yang, P. D.; Sun, Y.; Wu, Y.; Mayers, B.; Gates, B.; Yin, Y.; Kim, F.; Yan, H. *Adv. Mater.* **2003**, *15*, 353.
(9) Rao, C. N. R.; Deepak, F. L.; Gundiah, G.; Govindaraj, A. *Prog. Solid State Chem.* **2003**, *31*, 5.
(10) Rao, C. N. R.; Govindaraj, A. *RSC Nanoscience and Nanotechnology Series*; RSC Publishing: Cambridge, UK, 2005.
(11) Yang, R. S.; Chueh, Y. L.; Morber, J. R.; Snyder, R.; Chou, L. J.; Wang, Z. L. *Nano Lett.* **2007**, *7*, 269.
(12) Tenne, R. *Nat. Nanotechnol.* **2006**, *1*, 103.
(13) Wang, E. G. *J. Mater. Res.* **2006**, *21*, 2767.
(14) Peng, H. L.; Xie, C.; Schoen, D. T.; Mcllwrath, K.; Zhang, X. F.; Cui, Y. *Nano. Lett.* **2007**, *7*, 3734.
(15) Nian, J. N.; Teng, H. S. *J. Phys. Chem. B* **2005**, *109*, 10279.
(16) Sun, L.; Banhart, F.; Krasheninnikov, A. V.; Rodriguez-Manzo, J. A.; Terrones, M.; Ajayan, P. M. *Science* **2006**, *312*, 5777.
(17) Jiang, X. C.; Xiong, Q. H.; Nam, S.; Qian, F.; Li, Y.; Lieber, C. M. *Nano. Lett.* **2007**, *7*, 3214.
(18) Huang, M. H.; Mao, S.; Feick, H.; Yan, H. Q.; Wu, Y. Y.; King, H.; Weber, E.; Russo, R.; Yang, P. D. *Science* **2001**, *292*, 1897.
(19) Pan, Z. W.; Dai, Z. R.; Wang, Z. L. *Science* **2001**, *291*, 1947.
(20) Fang, X. S.; Zhang, L. D. *J. Mater. Sci. Technol.* **2006**, *22*, 721.
(21) Fang, X. S.; Gautam, U. K.; Bando, Y.; Dierre, B.; Sekiguchi, T.; Golberg, D. *J. Phys. Chem. C* **2008**, *112*, 4735.
(22) Schrier, J.; Demchenko, D. O.; Wang, L. W.; Alivisatos, A. P. *Nano. Lett.* **2007**, *7*, 2377.
(23) Hu, J. Q.; Bando, Y.; Liu, Z. W.; Sekiguchi, T.; Golbeg, D.; Zhan, J. H. *J. Am. Chem. Soc.* **2003**, *125*, 11306.
(24) Zhang, Y. F.; Yout, L. P.; Shan, X. A.; Wei, X. L.; Huo, H. B.; Xu, W. J.; Dai, L. *J. Phys. Chem. B* **2007**, *111*, 14343.
(25) Sun, X. H.; Sham, T. K.; Rosenberg, R. A.; Shenoy, G. K. *J. Phys. Chem. B* **2007**, *111*, 8475.
(26) Wang, Y. W.; Zhang, L. D.; Liang, C. H.; Wang, G. Z.; Peng, X. S. *Chem. Phys. Lett.* **2002**, *357*, 314.
(27) Borchers, C.; Stichtenoth, D.; Muller, S.; Schwen, D.; Ronning, C. *Nanotechnol.* **2006**, *17*, 1067.
(28) Fang, X. S.; Ye, C. H.; Zhang, L. D.; Wang, Y. H.; Wu, Y. C. *Adv. Funct. Mater.* **2005**, *15*, 63.
(29) Ye, C. H.; Fang, X. S.; Hao, Y. F.; Teng, X. M.; Zhang, L. D. *J. Phys. Chem. B* **2005**, *109*, 19758.
(30) Wang, H.; Liu, G.; Yang, W.; Lin, L.; Xie, Z.; Fang, J. Y.; An, L. *J. Phys. Chem. C* **2007**, *111*, 17169.
(31) Robinson, R. D.; Sadtler, B.; Demchenko, D. O.; Erdonmez, C. K.; Wang, L. W.; Alivisatos, A. P. *Science* **2007**, *317*, 355.
(32) Eymery, J.; Rieutord, F.; Favre-Nicolin, V.; Robach, O.; Niquet, Y.; Fröberg, L.; Mårtensson, T.; Samuleson, L. *Nano. Lett.* **2007**, *7*, 2596.
(33) Sekiguchi, T. *Mater. Res. Soc. Symp. Proc.* **2000**, *588*, 75.
(34) Djuri˘si'c, A. B.; Leung, Y. H. *Small* **2006**, *2*, 944.
(35) Greene, L. E.; Law, M.; Goldberger, J.; Kim, F.; Johnson, J. C.; Zhang, Y. F.; Saykally, R. J.; Yang, P. D. *Angew. Chem., Int. Ed.* **2003**, *42*, 3031.
(36) Jiang, Y.; Zhang, W. J.; Jie, J. S.; Meng, X. M.; Zapien, J. A.; Lee, S. T. *Adv. Mater.* **2006**, *18*, 1527.
(37) Yin, L. W.; Bando, Y.; Zhan, J. H.; Li, M. S.; Golberg, D. *Adv. Mater.* **2005**, *17*, 1972.
(38) Ye, C. H.; Fang, X. S.; Li, G. H.; Zhang, L. D. *Appl. Phys. Lett.* **2004**, *85*, 3035.
(39) Ye, C. H.; Fang, X. S.; Wang, M.; Zhang, L. D. *J. Appl. Phys.* **2006**, *99*, 063504.
(40) Li, C. P.; Lv, Y. Z.; Xu, H. B.; Ai, X. C.; Zhang, J. P. *J. Lumin.* **2007**, *122*, 415.
(41) Yuan, X. L.; Dierre, B.; Wang, J. B.; Zhang, B. P.; Sekiguchi, T. *J. Nanosci. Nanotechnol.* **2007**, *7*, 3323.
(42) Morozova, N. K.; Karetnikov, I. A.; Golub, K. V.; Danilevich, N. D.; Lisitsyn, V. M.; Oleshko, V. I. *Semiconductor* **2005**, *39*, 513.
(43) Akimoto, K.; Miyajima, T.; Mori, Y. *Phys. Rev. B* **1989**, *39*, 3138.

NL801353C